Pertanika J. Sci. & Technol. 33 (1): 441 - 464 (2025)

PERTANIKA JOURNALS

SCIENCE & TECHNOLOGY

Journal homepage: http://www.pertanika.upm.edu.my/

Synthesis and Assessment of Metal-Organic Frameworks (MOFs) Adsorbents for CO_2 Capture: A Comparative Work of the CO_2 Adsorption Capability of Mono- and Bimetal-based MOFs Adsorbents

Nor Khonisah Daud* and Nurul Huda Insyirah Muhammad Najib

Faculty of Chemical and Process Engineering Technology, Universiti Malaysia Pahang Al-Sultan Abdullah, Lebuh Persiaran Tun Khalil Yaakob, 26300 Kuantan, Pahang, Malaysia

ABSTRACT

Adsorption utilising porous solid adsorbent has been considered a feasible option for conventional CO_2 absorption over the past few decades. As a preliminary investigation towards obtaining Metal-Organic Frameworks (MOFs) adsorbent for CO_2 capture, the CO_2 adsorption efficiency using mono- and bimetal-based MOFs was assessed in this study. Among the numerous MOFs, Mg-MOF-74 exhibits the best CO_2 uptake at low pressures because of its open metal sites. A strategy to incorporate Zn in Mg-based MOF as a co-metal node is required to enhance the CO_2 adsorption performance of solid adsorbent. Selecting Zn as a metal node in MOF synthesis allows for the creation of stable, versatile, and functional materials for CO_2 adsorption. Therefore, combining several metals in a structure to develop a new MOF with an improved gas uptake is quite a useful approach to further harness the immense potential of MOFs. This study aims to compare the performance of mono- and bimetallic-MOFs and select the most suitable adsorbent for CO_2 capture. The performance of CO_2 adsorption was conducted using three parameters: the effect of metal loading on MOFs, pressure (1–5 bar) and adsorbent dosage (0.2–0.5g). Based on the characterisation findings, the studies confirm the formation of Mg-MOF-74, Zn-MOF and 50wt.%Zn/50wt.%Mg-MOF. Overall, it was found that the bimetal adsorbent with 50 wt.%Zn/50wt.%Mg-MOF displayed the highest CO_2 adsorption capacity (323 $mg_{CO2}/g_{adsorbent}$) when compared to the monometallic MOFs (Zn-MOF (134$mg_{CO2}/g_{adsorbent}$) and Mg-MOF-74) (122 $mg_{CO2}/g_{adsorbent}$) indicating a 50% increase in adsorption capacity over monometallic MOFs.

Keywords: Bimetal-based MOFs, CO_2 adsorption, metal-organic frameworks, mono-based MOFs, solid adsorbent

ARTICLE INFO

Article history:
Received: 21 March 2024
Accepted: 24 October 2024
Published: 27 January 2025

DOI: https://doi.org/10.47836/pjst.33.1.20

E-mail addresses:
khonisah@umpsa.edu.my (Nor Khonisah Daud)
nurulhudainsyirah98@gmail.com (Nurul Huda Insyirah Muhammad Najib)
*Corresponding author

ISSN: 0128-7680
e-ISSN: 2231-8526

INTRODUCTION

Solid adsorption has been identified as one of the most capable technologies for collecting or storing gas because of its low energy usage, importance to the environment and outstanding recyclability (Wang et al., 2016). The major driver in employing adsorption technology is to meticulously manufacture the appropriate permeable adsorbents. Of the under-studied adsorbents, comprising zeolites (Bao et al., 2011; Yang et al., 2013), porous carbons, Covalent-Organic Frameworks (COFs) (Li et al., 2015; Wang et al., 2014) and Hyper Cross-linking Polymers (HCPs) (Cui et al., 2017; Saha et al., 2017), Metal-Organic Frameworks (MOFs) are distinguished by their great surface area, modifiable pore size, and tuneable surface feature. With their nanoscopic pores and exceptionally superior surface areas, MOFs are outstanding substances for gas capture and storage. MOFs possess well-ordered and characterised permeable configurations and amendable chemical functionality that can be altered based on our requirements. Using various metal clusters and organic ligands, or both can also enhance the CO_2 selectivity of MOFs. An attentive selection of organic ligands and multi-metal units known as Secondary Building Units (SBUs) permit the assembly of MOF with the required properties and structural classes (Xin et al., 2011). Taking into account the capacity and usefulness of the carboxylate group, which illuminates strong co-ordination links and generates abundant structural patterns, organic multi-carboxylate ligands in various shapes, sizes, and rigidity/flexibility have been utilised to develop MOFs with diverse dimensions and varied topologies (Sumida et al., 2012). MOFs have been extensively examined for their ability to store and separate H_2, CH_4, CO_2, and hydrocarbons (Barea et al., 2014).

The combination of metal nodes in the framework of MOFs also enormously increases CO_2 adsorption by tuning and optimising the adsorptive properties and enhancing the electrostatic potential of the material. Of the known metal nodes, Mg and Zn are intensively investigated for CO_2 adsorption. It is mostly owing to the existence of open metal centres allowing themselves to be possible CO_2 adsorbents (Yu et al., 2012) and a thermally and chemically unchanging structure with extraordinary porosity (for example, huge volume of pores and surface area) which can be utilised as an appealing hosting material for *p* complexation adsorbents (Kim et al., 2018; Vo et al., 2019). Yazaydin et al. (2009) examined M-MOF-74 (M = Ni, Zn, Co, and Mg)'s capacity to adsorb CO_2 through simulation and experimental practices at 1 atm and 25^{o}C and Mg-MOF-74 showed the highest adsorption rate of CO_2, with a maximum of 8 mmol·g^{-1}. According to Bao et al. (2011), Mg-MOF-74 has a CO_2 intake much higher than zeolite 13X, reaching 8.61 mmol·g^{-1}. According to Tapiador et al. (2022), Zn-URJC-8 is a novel Zn-based MOF material that exhibits promising results in CO_2 conversion in added-value products. According to Zou et al. (2016), Zn-MOF showed an excellent ability to adsorb tiny molecular gases (CH_4, C_2H_6, and C_3H_8) and a remarkable ability to separate CO_2/CH_4, C_2H_6/CH_4, and C_3H_8/CH_4. At

273 K under 1 atm, this adsorbent can adsorb CO_2 at a rate of 92.1 $cm^3.g^{-1}$. Recent studies have concentrated on improving adsorbents and developing efficient processes to ensure profitable capture performance. Capturing and separating CO_2 from a large volume of flue gas is always costly and energy-intensive; consequently, more effective adsorbents need to be developed in relatively concentrated streams. The performance of adsorbents currently available for CO_2 capture technologies requires improvement in terms of adsorption capability, lifespan and multi-cycle sustainability. New high-efficiency adsorbents need to be developed to capture CO_2 in technologically efficient systems. Based on Mg-MOF-74 and Zn-MOF's excellent CO_2 adsorption capability, a bimetallic approach was proposed to enhance its CO_2 adsorption capability.

In bimetallic MOFs, two inorganic metallic nodes integrate two monometal MOFs. Bimetal MOFs significantly outperform their respective monometallic MOFs (Xie et al., 2020; Zhu et al., 2016) by using one-pot syntheses to produce them, which involve mixing various metals with appropriate ligands and linkers or by implementing post-synthetic changes by dipping a monometal MOF into a concentrated solution of a diverse (but compatible) metallic ion. These bi-metal MOFs have synergic effects and enhanced properties over their monumental counterparts, such as better adsorptive selectivity, selective catalysation and structural stability. Whereas Mg-MOF-74 bimetal is used extensively in thermocatalysis (Gao et al., 2021; Zurrer et al., 2021), its use in CO_2 adsorption is limited. Zhang et al. (2022) reported on mercury removal using bimetallic iron-copper-based Metal-Organic Frameworks (Fe-Cu-MOFs). The analysis of adsorption kinetics indicates that Fe-Cu-MOFs have a mercury equilibrium adsorption capability of 12.27 $mg.g^{-1}$. Kaur et al. (2016) presented the findings of the formulation of Co-Zn–ZIF-8 bimetal adsorbents. The incorporation of Co^{2+} resulted in a 33% increase in pore volume and a 40% increase in surface area through their work. Co-Zn-ZIF-8 bimetal adsorbents also exhibited increased CO_2 adsorption under environmental conditions. These findings confirmed the advantages of synthesising bi-Metal Organic Frameworks for the development of MOF applications. Ling et al. (2022) stated that Mg_xCu_{1-x}-MOF-74's CO_2 adsorption capability was exceptional when prepared at 398 K and for 24 hours in the dimethyl-formamide (DMF)-EtOH-MeOH mixture's solvents. The CO_2 sorption of $Mg_{0.4}Cu_{0.6}$-MOF-74 increased the most when exposed to an Xe lamp for 24 hours, reaching 3.52 $mmol.g^{-1}$. It surpassed that of Mg- and Cu-MOF-74 by 1.18 and 2.09 times, respectively. The interaction between Mg and Cu metals resulted in a stronger photostability of Mg_xCu_{1-x}-MOF-74 for CO_2 uptake and a wider range of photocatalytic applications. The "bimetal" approach has significant potential for usage in MOFs and provides an achievable adsorbent design method with outstanding CO_2 adsorption capability.

Within this context, this work presents the findings of a comparative study of the CO_2 adsorption efficiency of mono- and bimetal-based MOF adsorbents in the post-

combustion process to understand the CO_2 adsorption performance of MOFs when employed as solid adsorbents for the purpose of capturing CO_2. The results documented in this study could help optimise the CO_2 adsorption capability of MOF for CO_2 capture.

METHODOLOGY

Materials

The selected adsorbents were synthesised using magnesium nitrate hexahydrate Mg $(NO_3)_2 \cdot 6H_2O$, 2,5-dihydroxyterephthalic acid, Dimethylformamide (DMF), ethanol, methanol, Zn $(NO_3)_2 \cdot 6H_2O$, CO_2 and deionised water. The chemicals were procured from Capital Eng. Resource Sdn Bhd was used directly in the experiments without additional purification.

Formulation of Adsorbents

Formulation of Mg-MOF-74, Zn-MOF and Mg/Zn-MOF

The Mg-MOF-74 adsorbent was produced employing the impregnation approach by dissolving 2,5-dihydroxyterephthalic acid into 12 mL of ethanol at an ambient condition. Subsequently, 0.795 g of magnesium nitrate hexahydrate in 12 mL of water was added into the synthesised mixture to develop Mg-MOF-74, followed by continuously stirring and drying to 120°C overnight. The powder was calculated in a furnace at 200°C for 1 hour. This method was repeated by changing 0.795 g of Zn $(NO_3)_2 \cdot 6H_2O$ to 12 mL of water as the metal group for MOF.

In the case of bimetallic adsorbent, the specific amounts of magnesium nitrate hexahydrate and Zn $(NO_3)_2 \cdot 6H_2O$ (15–85 wt.% of metal ions in MOF) were dissolved in a beaker containing 12 mL of deionised water. Then, 2,5-dihydroxyterephthalic acid in 12 mL of ethanol was mixed into this aqueous mixture and was stirred constantly on the hot plate until the mixture mixed well. After impregnation, the samples were dried at 120°C for 12 hours before being calcined at 200°C for one hour in a muffle furnace.

Structural Characterisations

Information on powdered XRD from different adsorbents was gathered by Geigerflex (Rigaku, Inc) diffractometer employing Cu Kα radiation (0.154 nm) with scanning between 5.00 and 40.00 (2h) (variables: voltage (45 kV), current (35 mA), step size (0.020), and 1.2 min^{-1}). SEM pictures were acquired by means of a Hitachi S-2600 N scanning electron microscopy. The EDX analyses were done using the same instrument and parameter as the SEM at two different locations using the images obtained from SEM analyses. A Bruker Vector 22 FTIR spectrometer was employed to collect FTIR spectra within the frequency limit of 4000-500 cm^{-1}. N_2 adsorption/desorption isotherms were achieved at 77 K on a

Coulter CX-300 adsorption device. The specimen was degassed at 105°C for 24 hours by means of a high vacuum line before N_2 adsorption. The BET surface area was defined in the P/P_0 limit from 0.02 to 0.25 since the pores were occupied at extremely low relative pressure.

Gas Sorption Measurements

As shown in Figure 1, a cylindrical metal vessel was used as a device to perform the gas sorption process. This device was connected to the flow lines of CO_2 and N_2 tanks. Before the adsorption process started, N_2 gas was flowing to purge out all the impure components in the device. After the purging, the CO_2 valve was opened and led to fill in the device. The concentration of pure CO_2 gas was collected first without adsorbents in the device to attain the concentration of pure CO_2. Before setting the operating temperature and pressure, the device was loaded with the required amount of adsorbent. After the adsorbent was loaded into the device, CO_2 flowed and achieved the required pressure, and the CO_2 adsorption process took place.

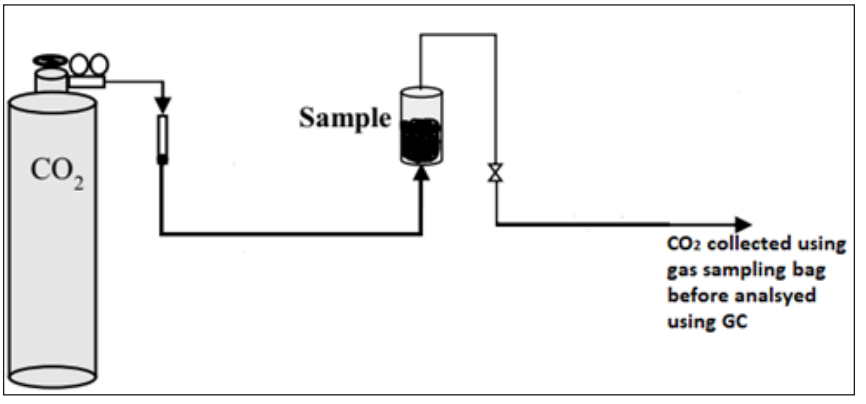

Figure 1. A schematic diagram of the CO_2 adsorption test set-up

The exit gas was collected using a gas sampling bag to determine the total CO_2 adsorbed onto the adsorbent during a specific time interval, and the concentration was identified using Agilent 6890 FID gas chromatography. The amount of CO_2 sorbed over a given timespan was determined using Equation 1:

$$q_t = \frac{(C_o - C_t)V}{m} \quad [1]$$

where q_t, C, V and m are the quantity of CO_2 sorbed per dosage of adsorbent ($mg.g^{-1}$), CO_2 concentration, volume of the device (L) and dosage of the adsorbent (g), respectively.

The subscripts *o* and *t* indicate the conditions at the initial and CO_2 concentrations at interval time.

Effect of Pressure

CO_2 adsorption was run at 0.2 g of adsorbent amount, ambient temperature, and 50 wt.% Mg/50 wt.% Zn-MOF of metal loadings to study the influence of adsorption pressure (1–5 bar).

Effect of Amount of Adsorbent

The study examined the effect of the amount of adsorbent on CO_2 uptake by varying the amount used (0.2, 0.3, 0.4 and 0.5 g) while maintaining pressure, temperature, and metal loading on MOF constant at 5 bar, ambient temperature and 50 wt.% Mg/50 wt.% Zn-MOF, respectively. The CO_2 adsorption was run in the reactor and analysed periodically.

Effect of Metal Ions Loading on MOF Adsorbent

The CO_2 adsorption process involved studying the impact of metal ion loading on the MOF. Different metal ion loadings (15–85 wt.%) for Mg and Zn were added along with CO_2 gas. The experiment's parameters were maintained at the optimum level of adsorbent dosage and pressure.

RESULTS AND DISCUSSION

Characterisation of the Prepared Adsorbents

Crystallographic Structure and Chemical Composition Analysis

Apart from the particles' specific surface area, the crystallinity of particles plays a role in CO_2 adsorption. Understanding the crystallinity of a material through crystallographic structure analysis provides valuable insights into its structural properties, which in turn affect its adsorption behaviour (Lee et al., 2012). Figure 2 indicates that the diffraction profile of Mg-MOF-74 was well aligned with the work described in the previous study (Campbell & Tokay, 2017). The blue line showed characteristic peaks at 15.60° (101) and 20.30° (202), confirming the formation of Mg-MOF-74. The existence of these distinctive bands, together with the presence of magnesium nitrate hydrate in the adsorbent, indicate that Mg-MOF-74 has been successfully formulated. The XRD pattern agreed with the Powder Diffraction Files (PDFs) (Reference No. 00-001-0349). Additionally, the crystalline structure of Mg-MOF-74 is confirmed by the sharp bands in this pattern. Crystalline structure tends to be more stable thermally and chemically, which can be advantageous in adsorption processes that involve harsh conditions. This crystalline material might have specific, high-energy sites that can strongly bind adsorbates (Lee et al., 2012).

The main peaks of the diffraction scheme for Zn-MOF (orange line) were obtained at 2 θ values of around 11.05° (022), 13.58° (001), 16.70° (013), 19.10° (111), 25.40° (002), 28.90° (100) and 30.40° (044) that correspond to simulated XRD patterns, proving that the structure complies with the studies that have been reported (Bagheri et al., 2018; Li, 2021). Based on Figure 2, high-intensity peaks were indicating the crystallinity of Zn-MOF. The phase identification of the sample shows zinc nitrate hydroxide was identified as the main phase in Zn-MOF (PDF reference No. 04-014-0671).

The XRD patterns of 50 wt.% Mg/50 wt.% Zn-MOF (grey line) were well in line with those of Mg- or Zn-MOF. 50 wt.% Mg/50 wt.% Zn-MOF exhibited significant diffraction bands at 2θ = 13.30° (100), 20.55° (202), 21.90° (100), 25.52° (012), 27.60° (002), 33.10° (101) and 36.60° (012), which match those of the reported MOF-74 (Kahr et al., 2013; Tan et al., 2014). The phase identification of the sample 50 wt.% Mg/50 wt.% Zn-MOF shows a combination of more than one phase, with main phases of magnesium nitrate hydrate (PDF reference No. 00-001-0349) and zinc nitrate hydroxide (PDF reference No. 04-014-0671) developing from the co-ordination reaction of Mg, Zn, and DMF (Li et al., 2021). The replacement of Mg by Zn has no impact on the crystalline structure of Mg-MOF-74 or Zn-MOF, and 50 wt.% Mg/50 wt.% Zn-MOF is successfully synthesised.

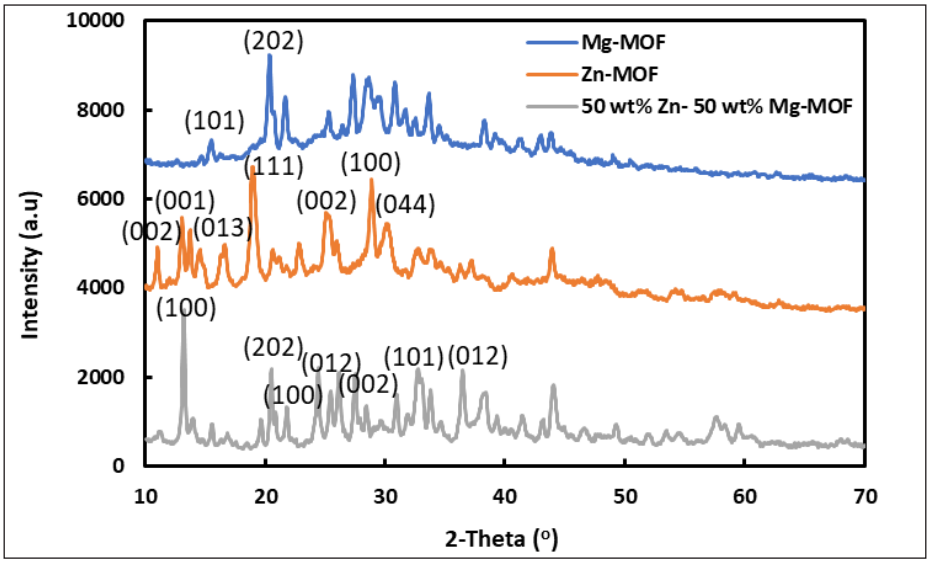

Figure 2. XRD patterns of Mg-MOF-74, Zn-MOF and 50 wt.% Zn/50 wt.% Mg-MOF

Surface Functional Group Analysis

This analysis was carried out to discover the surface functional groups of single and bimetallic adsorbents, as shown in Figure 3 and Table 1. All vibrations can be separated into two distinct zones based on the MOF's co-ordination characteristics (Abooali et al.,

2020; Romero-Muñiz et al., 2020). The characteristic vibrations over the 700 cm^{-1} zone are organic ligands, and regions under 700 cm^{-1} have their place primarily in the metallic centres of Mg and Zn (Abooali et al., 2020)—the findings of Mg-MOF-74 (blue line), Zn-MOF (orange line) and 50 wt.% Mg/50 wt.% Zn-MOF (grey line) show a significant peak at 3369.19, 3233.49, 3483.57, 3346.10 and 3241.15 cm^{-1} which are attributable to the hydroxyl group of H-bonded OH broad stretching. Moreover, the absorption bands at 2411.19, 2364.30, 2360.82, 2193.70, 2123.58, 2191.64, 2161.60, 2113.03, 2081.92, 2007.90, 1994.76, 1988.95, 1944.88, 1963.16, 1779.05, 1647.56, 1646.90, 1624.93, 1577.57 and 1550.32 cm^{-1} appeared in the Mg-MOF-74, Zn-MOF and bimetal 50 wt.% Mg/50 wt.% Zn-MOF were ascribed to the vibration modes in the nitrile bond C≡N, O-H stretching vibrations caused by the intermolecular hydrogen bond of polymer compounds such as alcohols, phenols and carboxylic acid as well as aromatic C=C in-plane deformations peaks. A nitrile functional group C≡N is derived from DMF solvent (Heravi et al., 2018). A number of sharp and clear absorption bands were detected at 1491.85, 1375.52, 1341.25, 1311.79, 1051.71, 1038.78, 1024.28, 1011.22, 819.05, 818.58, 804.31, 803.29 and 730.07 cm^{-1}, that were assigned to ν(−C=O), ν(−COO−), and ν(C–H) of benzene rings (Abooali et al., 2020; Gao et al., 2021). Carboxylic functional groups found in adsorbents contribute to the 'breathing effect' as an outcome of the intra-framework interaction, which improves the CO_2 adsorption capability of the adsorbent (Serre et al., 2007). The characteristic peaks at 580 and 373 cm^{-1} could be referred to as the metal cations, Mg^{2+} and Zn^{2+} in the Mg-MOF-74, Zn-MOF and 50 wt.% Mg/50 wt.% Zn-MOF (Wang et al., 2021). All adsorbents

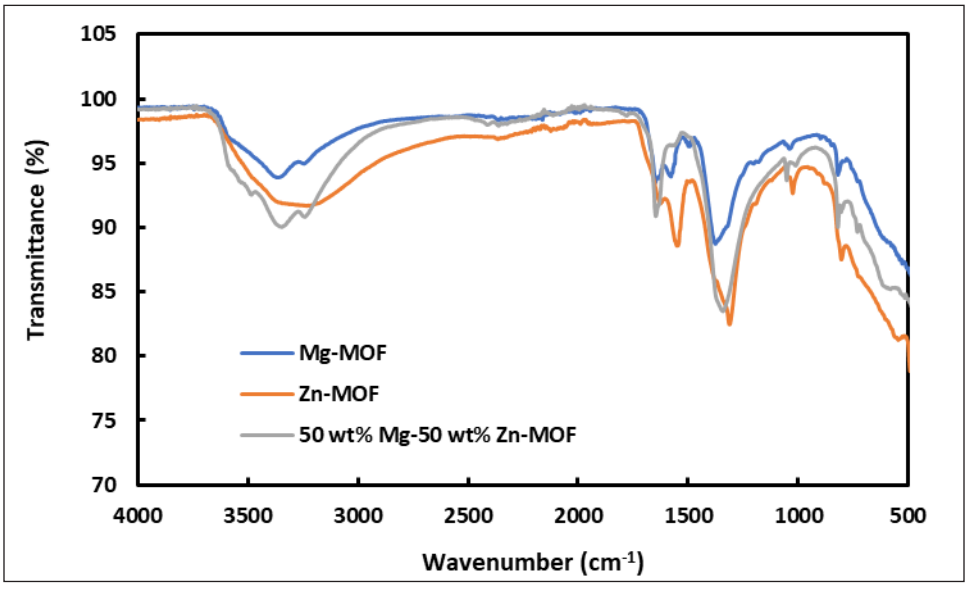

Figure 3. Surface functional group patterns of Mg-MOF-74, Zn-MOF and 50 wt.% Zn/50 wt.% Mg-MOF

obtained exhibit the aforementioned characteristic peaks (Figure 3) (Li et al., 2021), which proves that Mg-MOF-74, Zn-MOF and 50 wt.% Mg/50 wt.% Zn-MOF crystals were successfully synthesised.

Table 1
Wavenumber of Mg-MOF-74, Zn-MOF and 50 wt.% Mg/50 wt.% Zn-MOF adsorbents

Wavenumber (cm-1)			
Mg-MOF-74	**Zn-MOF**	**50 wt.% Mg/50 wt.% Zn-MOF**	**Functional Group**
3369.19	3233.49	3483.57	Hydroxyl (O-H)
		3346.10	
2360.82	2364.30	3241.15	Carboxylic Acid (O-H), C≡N, C=C
2191.64	2193.70	2411.19	
2161.60	2123.58	2360.48	
2081.92	1988.95	2113.03	
2007.90	1936.16	1994.76	
1944.88	1624.93	1779.05	
1647.56	1550.32	1646.90	
1577.57			
1491.85	1311.79	1341.25	ν(−C=O), ν(−COO−), and ν(C–H)
1375.52	1024.28	1051.71	
1038.78	803.29	1011.22	
819.05		818.58	
		804.31	
		730.07	
580.00		580.00	Mg-O
	373.00	373.00	Zn-O

Surface Morphology Analysis

The morphology of single and bimetallic 50 wt.% Mg/50 wt.% Zn-MOF were analysed through a Scanning Electron Microscope (SEM) analyser at different magnifications, as displayed in Figure 4. As indicated by Figure 4, there is a notable contrast in the surface morphology of the adsorbents. Irregular and favourably porous networks full of pores, flaws, and cracks are seen in the Mg-MOF-74 images (Figures 4(a) and (b)). The produced Mg-MOF-74 has a few voids attributed to the devolatilisation of inorganic materials primarily attached to the adsorbent wall. The images displayed in Figures 4(c) and (d) reveal Zn-MOF with a rough surface and some agglomerations. Figures 4(e) and (f) clearly demonstrate that 50 wt.% Mg/50 wt.% Zn-MOF's morphology has a similarity to those of the reference adsorbents but with an extra coral reef-like structure after the Zn^{2+} ions were introduced into the Mg-MOF-74. Therefore, the morphology of MOFs was significantly influenced by the presence of Zn^{2+} in the reaction solution, which is similar to that in a previous report by Yang et al. (2014).

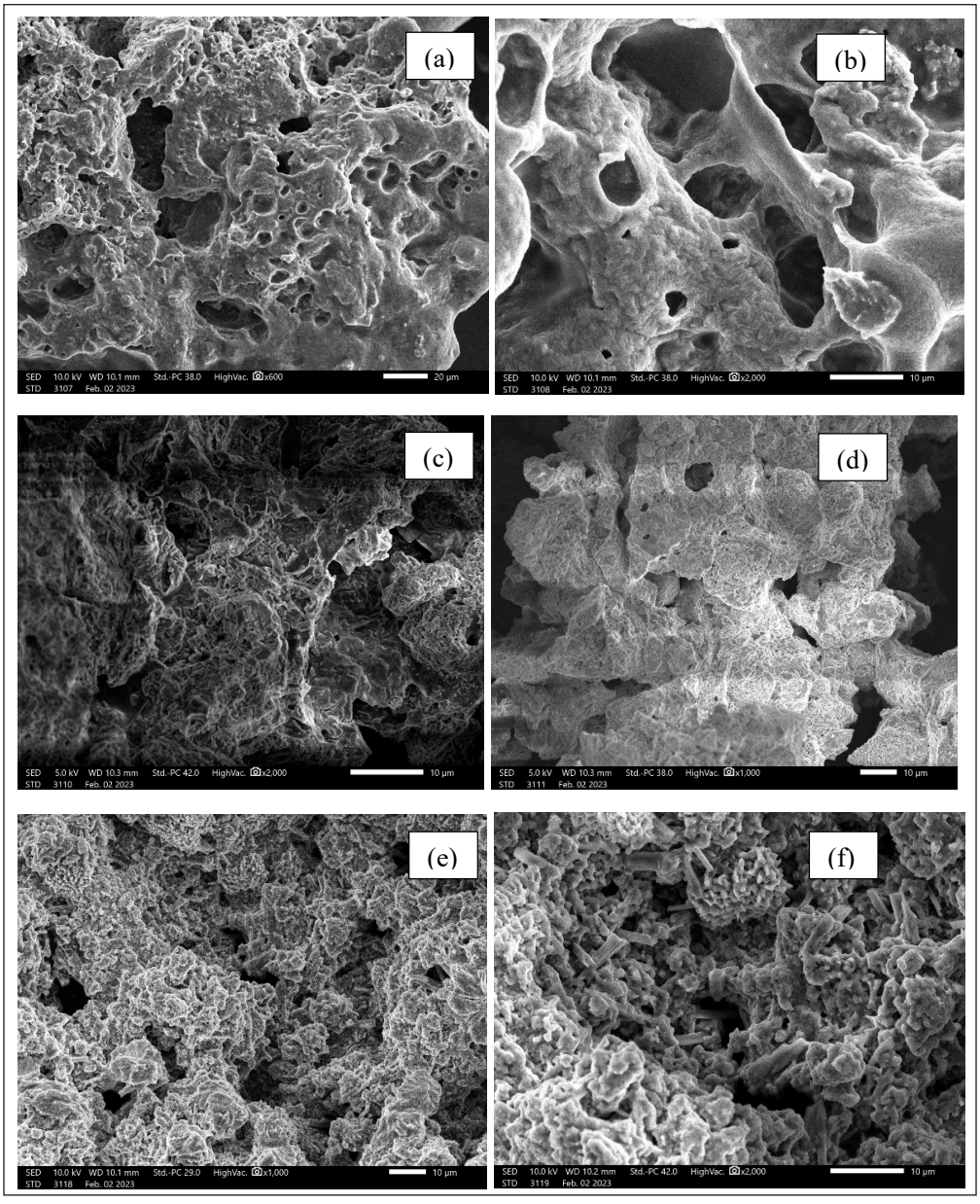

Figure 4. SEM pictures for (a) Mg-MOF-74 (Magnification = 600x), (b) Mg-MOF-74 (Magnification = 2000x), (c) Zn-MOF (Magnification = 2000x), (d) Zn-MOF (Magnification = 1000x), (e) 50 wt.% Zn/50 wt.% Mg-MOF (Magnification = 1000x), and (f) 50 wt.% Zn/50 wt.% Mg-MOF (Magnification = 2000x)

Elemental Composition Analysis

The dissemination of the major components in the mono- and bi-metal 50 wt.% Mg/50 wt.% Zn-MOF was investigated by performing elemental composition analysis employing

an energy-dispersive X-ray analyser (EDX), and the results are shown in Table 2. The findings propose that the major components in the single (Zn-MOF and Mg-MOF-74) and bimetallic 50 wt.% Mg/50 wt.% Zn-MOF adsorbents, including Mg, Zn, C, and O, are uniformly distributed on the exterior of the solid materials. These well-distributed components offer significant active spots for CO_2 adsorption.

Table 2
Chemical Composition of Zn-MOF, Mg-MOF-74, and 50 wt.% Mg/50 wt.% Zn-*MOF*

Elements	**Mass (%)**		
	Mg-MOF-74	**Zn-MOF**	**50 wt.% Zn/50 wt.% Mg-MOF**
O	69.13	41.73	59.37
Mg	15.26	-	7.64
C	15.60	11.77	4.4
Zn	-	46.50	28.59

Surface Area Analysis

The N_2 adsorption-desorption multipoint was used to evaluate the N_2 physisorption isotherms of the synthesised adsorbents at 77 K. The findings are depicted in Figure 5. According to the IUPAC class, the isotherms of all adsorbents are in category IV and have an H3 hysteresis loop that shows the occurrence of mesoporosity within all prepared adsorbents. Table 3 presents the samples' surface area, pore volume, and average pore size. CO_2 loading onto adsorbents is mediated through physical adsorption, which largely determines its adsorption by characteristics such as specific surface area and crystallinity (Lee et al., 2012). Comparatively, 50 wt.% Mg/50 wt.% Zn-MOF has a larger specific surface area than other adsorbents. This may be due to more mesopore structures and smaller crystal sizes in this material. The large surface area facilitates CO_2 uptake. In Table 3, the surface area is 50 wt.% Mg/50 wt.% Zn-MOF was approximately 3.13% bigger than that of Zn-MOF and 0.86% bigger than that of Mg-MOF-74. Zn-MOF had the minimum surface area and mesopore volume. This finding is consistent with the previous reports by Ling et al. (2022), Li et al. (2021) and Sun et al. (2019). The increase in specific surface area of 50 wt.% Mg/50 wt.% Zn-MOF can be attributed to the slight difference in cation radius and co-ordination modes between Mg and Zn cations. When constructing infinite structural units, bimetallic structures increase porosity and surface area. Present results are consistent with those expected because heavier transition metal substitution increases surface area (Villajos et al., 2015). Considering the double atomic mass of Zn with respect to Mg, the increase of surface area by bimetallic co-ordination in MOFs should be higher in terms of molar equivalent. It is thought that more vacancies might be created in the framework when a second metal ion was introduced, which includes lattice distortion

and locally unbalanced co-ordination, consequently resulting in higher porosity or higher lamellar charge (Vuong et al., 2013).

Notably, many MOF-74 have been reported with BET surface areas of more than 700 m^2/g, with the highest surface area reported for MOF-74 approaching 1900 m^2/g. While the surface areas of these prepared adsorbents fall short of the highest values achieved for MOF-74, this suggests that the comparatively low surface areas measured to date for prepared adsorbents are not an inherent limitation of their molecular nature. Following solvent exchange during the preparation of MOF materials, activation protocols that circumvent material decomposition and ensure complete removal of solvent guests are critical. Because the open metal sites in MOFs are of paramount importance for CO_2 adsorption, it is critical to completely free the metal sites of bound solvent during activation. If these methods are not performed properly, activation can cause structural collapse, thereby diminishing porosity and reducing material surface area (Deegan et al., 2021). In this study, the BET surface areas for all prepared adsorbents appear quite low; this might be due to the employment of temperature during the activation process (~200°C), below the optimum temperature for DMF removal. Valenzano et al. (2011) showed via IR and EXAFS that dehydration of the Zr-cluster begins upon activation at 250°C and was completed at 300°C. The IR data indicated that the material was free of DMF by 250°C, indicating that this was the optimal activation temperature for solvent removal without changing the material structure. Indeed, this produces a high surface area of 1187 m^2/g.

Figure 5 shows the isotherm linear plot for CO_2 adsorption and desorption of different prepared adsorbent samples. According to the IUPAC classification (Kahr et al., 2013), pores are classified into mesopores with pore diameters in the range of 2 to 50 nm. Table 3 reveals that all adsorbents have pores ranging in size from 2.6 to 6.5 nm. In addition,

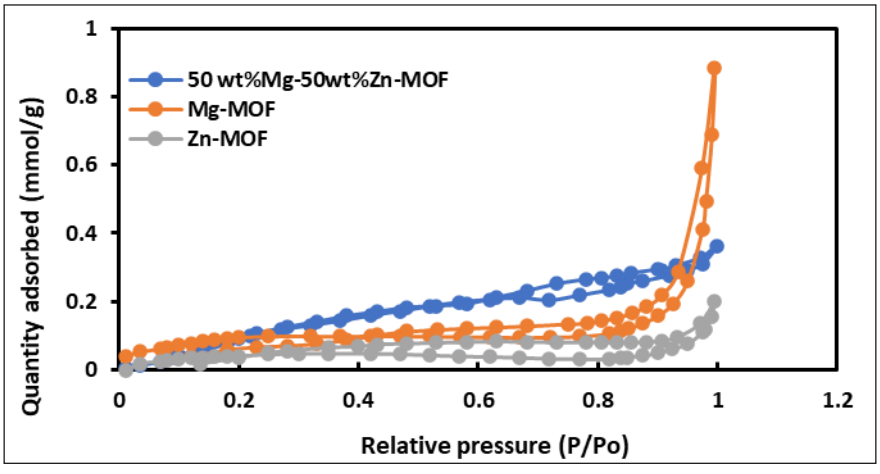

Figure 5. N_2 adsorption/desorption isotherms for Zn-MOF, Mg-MOF-74 and 50 wt% Zn/50 wt% Mg-MOF

as expected, the smaller pore size of 50 wt.% Mg/50 wt.% Zn-MOF relative to parental adsorbents is apparent.

Table 3
Textural parameters for Zn-MOF, Mg-MOF-74 and 50 wt.% Zn/50 wt.% Mg-MOF attained from the N_2 adsorption isotherm at 77 K

Sample	BET surface area (m2g-1)	Pore size (Å)	Pore volume (cm3g-1)
50 wt.% Zn/50 wt.% Mg-MOF	16.1695	26.6103	0.010757
Mg-MOF-74	8.7069	65.5707	0.014273
Zn-MOF	3.9186	38.5605	0.003778

CO_2 Adsorption

Influence of Different Metal Loading on MOF

The ability of single and bimetallic MOFs to adsorb CO_2 was assessed through the CO_2 adsorption analysis approach. The quantity of adsorbed CO_2 was determined per analysis, and the CO_2 adsorption value was employed to assess the performance of various adsorbents. Figure 6 illustrates the CO_2 adsorption capabilities of bi-metal MOF and pristine MOF. Since these adsorbents can be prepared fairly easily, and the metals studied to ensure that the characteristic properties of the MOF are preserved, like crystalline structure, thermal stability, and comparatively high surface area, it is therefore vital to investigate the ability of these materials to adsorb CO_2. As can be seen in Figure 6, it is notable that the Zn-MOF and Mg-MOF-74 are capable of obtaining CO_2 at 134.55 and 122.08 mg/g, respectively, but bimetallic MOF has significantly higher adsorption capacities. In this present study, an Mg-MOF-74 acts as a parent structure and exhibits excellent CO_2 adsorption under ambient temperature and mild pressure conditions. However, adding another metal ion, such as Zn^{2+}, as the bimetallic strategy is feasible for adsorbent design to achieve remarkable CO_2 adsorption capacity in the future. In principle, it is thought that mixed-metal MOFs can offer several advantages over monometallic MOFs by providing complexity and introducing functionality derived from the different metal ions in the MOF structure, and it is predicted that the adsorption performance of bimetal MOFs will be beyond that achieved by homometallic MOFs (Abednatanzi et al., 2019; Masoomi et al., 2019). In this study, the impregnation method was employed to synthesise the adsorbents where MOFs were constructed with two main components: the metal inorganic clusters and the organic linkers, where the linkers acting as "struts" connect the "joints" of metal ions (Abednatanzi et al., 2019). Usually, organic linkers are the processing targets to design functional MOFs to boost adsorption performance; for example, adopting large organic linkers enables larger pore size of MOFs to facilitate adsorption diffusion (Vuong et al., 2013), and decorating organic linkers with targeted groups [-NH_2 (Howarth et al., 2015), -OH (Luo et al., 2015)] offers more effective sites to increase adsorption capacity or improve adsorption selectivity.

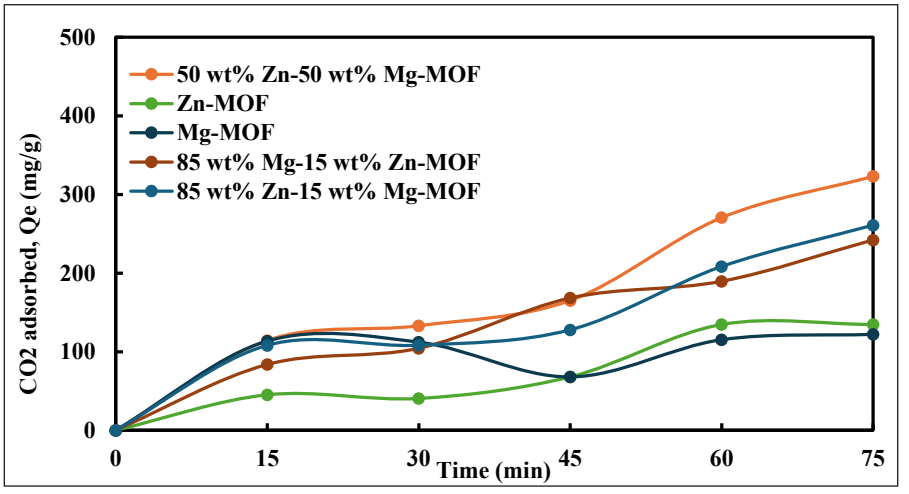

Figure 6. Influence of metal loading on MOFs. Initial conditions: pressure = 5 bar, adsorbent dosage = 0.3 g, initial concentration of CO_2 = 637 ppm and ambient temperature

Almost all bimetallic MOFs with different percentages of metal loading exhibit a greater adsorption capacity than single MOFs. Adsorption capacity soars in the direction Mg-MOF-74 < Zn-MOF< 85 wt.% Mg/15 wt.% Zn-MOF < 85 wt.% Zn/15 wt.% Mg-MOF<50 wt.% Zn/50 wt.% Mg-MOF, reaching, accordingly, 122.08 mg/g, 134.55 mg/g, 242.14 mg/g, 260.85 mg/g and 323.21 mg/g. 50 wt.% Zn/50 wt.% Mg-MOF shows an increased CO_2 adsorption capacity over all MOFs prepared in this study. This phenomenon could be attributed to the surface area and the pore volume of the adsorbent since the specific surface area is 50 wt.% Zn/50 wt.% Mg-MOF (16.1695 m^2/g) is larger than that of Mg-MOF-74 and Zn-MOF (8.7069 m^2/g and 3.9186 m^2/g, respectively). Mesoporosity is a characteristic of single and bimetallic MOFs that may be indicative of successful adsorbent formation. Mesoporous materials are also believed to support CO_2 adsorption because the bimetal (Zn and Mg) that were mixed to MOF was not clogging the pores of pristine MOF itself, thereby enhancing the quantity of porosity in the bimetallic MOF. The adsorption capacity of a single MOF (Zn-MOF or Mg-MOF-74) is relatively high, whereas as the metal substance rises to 50 wt.% and over 85 wt.%, the adsorptive capability of the MOF drops substantially. This tendency, in turn, may be described by the amount of metal loading too much, which lowers adsorbent porosity by plugging some of the MOF's pores. The availability of adsorption sites decreases, which affects the potential for CO_2 sorption. According to the reported literature (Liu et al., 2019; Ren et al., 2020; Szczesniak et al., 2018; Wu et al., 2010), CO_2 adsorption may initially occur on open Zn or Mg cations and MOF cage windows, subsequently through further adsorption induced by van der Waals forces. The electrostatic interaction between Zn or Mg cations and CO_2 quadrupole is more significant than the van der Waals interaction. The addition of metals

in MOF, such as Zn or Mg, that contain oxygen-functional groups has been supported by mesopores structures particularly favourable for diffusion and mass transfer, probably because of the co-ordination linkages between the oxygen functional groups and Mg or Zn in the MOF structure.

Furthermore, the findings show that the metals used and their added quantity are significant in the MOF. For instance, 50 wt.% Zn/50 wt.% Mg-MOF has a higher adsorption capacity than Mg-MOF-74 and Zn-MOF, and the addition of metals and loading leads to a substantial rise in capacity relative to pristine MOF. Taking into account both the Mg and Zn content in MOF (ranging from 15 to 50 wt.%) and the CO_2 adsorption capability of pristine MOF, it might be inferred that the CO_2 uptake of bimetallic MOF is improved. Moreover, the Zn content influenced the CO_2 adsorption capacity of bimetal-based MOF. With the decrease in the Zn content, the CO_2 uptake of bimetal-based MOF decreased, which was attributed to the CO_2 adsorption heat of Zn ions being larger than that of Mg ions in a mild-pressure region. Because of the synergistic effect between Zn and Mg, the CO_2 adsorption of bimetallic-based MOF was enhanced considerably. These findings are in good agreement with the results obtained when Co and Zn coexist in the MOF-74 structure (Botas et al., 2011). So, a synergetic effect between Mg and Zn metal cations and the pore size reduction may contribute to CO_2 molecules retention with higher energies in this material. This fact can be explained as a result of Coulombic interaction forces related to the proximity of CO_2 to the adsorbent and the reduced pore diameter in this material (Zhou et al., 2008). So, the presence of a certain amount of Zn in Mg-MOF-74 material enhances the CO_2 adsorption capacity and energy interaction strength onto this framework, rather than having pure zinc or magnesium clusters, possibly as a consequence of the electronic environment that attracts slightly stronger CO_2 molecules as well as the differences in textural properties among isostructural materials or even to the presence of defects in the crystal structure that restrict the access to some of the pores (Sillar & Sauer, 2012). Adding bimetallic is vital, but it is crucial to keep in mind that the quantity of added metal is significant. The greater its content, the lower the porosity and adsorption capability of the CO_2.

In general, one can conclude that sorbents are the most promising at 50 wt.% Zn/50 wt.% Mg-MOF, which shows the highest CO_2 adsorption capacity.

Impact of Operating Pressure

Pressure plays a crucial role in the performance of the solid adsorbent in practical applications; hence, the effect of pressure was examined and depicted in Figure 7.

Various operating pressures were used to determine the amount of CO_2 adsorbed during 75 minutes of adsorption time, and the findings exhibit that it increases from 195.63 mg/g to 438.91 mg/g from 1 bar to 5 bar operating pressure. The rise in CO_2 uptake is attributed

to increased gas particles hitting the adsorbent surface, caused by the rising pressure. The openings are filled with CO_2 molecules as a result of higher pressure. The remarkable enhancement in CO_2 adsorption capability observed can be attributed to the synergetic effect of high P: high pressure effectively modifies the pore size and shape via changing the linker orientation and creating new adsorption sites within MOF. More significantly, several studies have shown that application of high external pressure can effectively tune CO_2 storage capability in MOFs (Choi et al., 2019; Hu et al., 2013, 2015; Jiang et al., 2018; Kontos et al., 2020). External pressure can change the MOF framework topology, alter pore size and shape, enhance host-guest interactions between framework and adsorbed CO_2, and even create new adsorption sites, increasing CO_2 adsorptive capability. High mechanical pressure changes the effective pore size and shape as well as the linker orientation to open the "gate", facilitating the CO_2 adsorption. The change in the linker orientation also makes the channels connecting the cages accessible to CO_2 as additional adsorption sites at high pressure. The substantial difference in adsorptive capacity improvement under different pressures is intriguing and can be closely attributed to the framework structure under different pressures. Previous work by Moggach et al. (2009) showed that high external pressure could increase the effective pore size of MOFs by changing the linker orientation, which is the so-called "gate opening" effect.

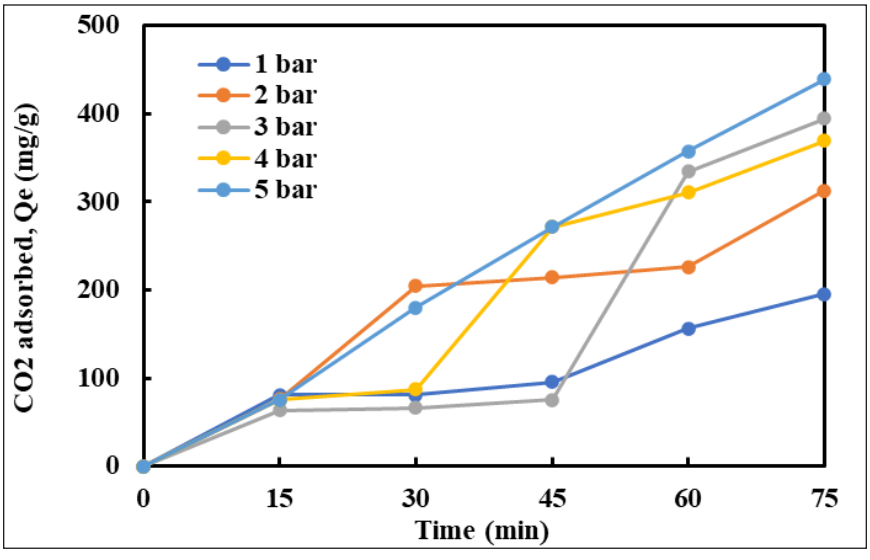

Figure 7. Influence of pressure on CO_2 uptake. Initial condition: adsorbent dosage = 0.4 g adsorbent, initial concentration of CO_2 = 637 ppm, metal loading = 50 wt.% Zn/50 wt.% Mg-MOF and ambient temperature

However, at room temperature, the solidification of CO_2 occurs at a pressure above 0.6 GPa (Giordano et al., 2006). This phase change of CO_2 severely limits further insertion of CO_2 into the cavities of MOFs at higher pressures since solid CO_2 is immobile and not

diffusible. This problem can be remediated if a mixture of solid CO_2 and MOFs is heated to a temperature at which solid CO_2 existing outside MOFs is mobilised so that a significantly larger number of CO_2 molecules may be pressed into the framework of MOFs by pressure. Consequently, the CO_2 vibrations appeared at higher frequencies. A possible reason is that the framework might have been partially damaged by exposing the MOFs to harsher conditions, resulting in a slightly reduced porosity for adsorption.

It can be concluded that the increase in working pressure affects the formulated adsorbent's CO_2 adsorption, contrasting the findings of CO_2 adsorption by employing various working pressures (Figure 7). In addition, the capability of samples to adsorb CO_2 is highly subject to factors such as surface area, pore size and pore volume. The form of the isotherm shows the resulting 50 wt.% Zn/50 wt.% Mg-MOF is a mesoporous structure with the greatest surface area (16.1965 m^2/g) (Table 3). The presence of more active sites is increased due to increased surface area and pressure, directing towards greater adsorption of CO_2. Furthermore, the surface area significantly influences CO_2 adsorption uptake (Chen et al., 2017). It is apparent that other aspects are impacting CO_2 uptake.

Effect of Dosage of Adsorbent

Figure 8 exhibits the effect of changing the dosages of 50 wt.% Zn/50 wt.% Mg-MOF from 0.2 to 0.5 g on CO_2 adsorption process. Based on the findings presented in Figure 8, 0.3 g should be the optimum dosage for CO_2 uptake as it has the utmost CO_2 adsorption capacity at 740.90 mg/g. Expanding the dosage up to 0.5 g reduced the adsorption capacity by 54

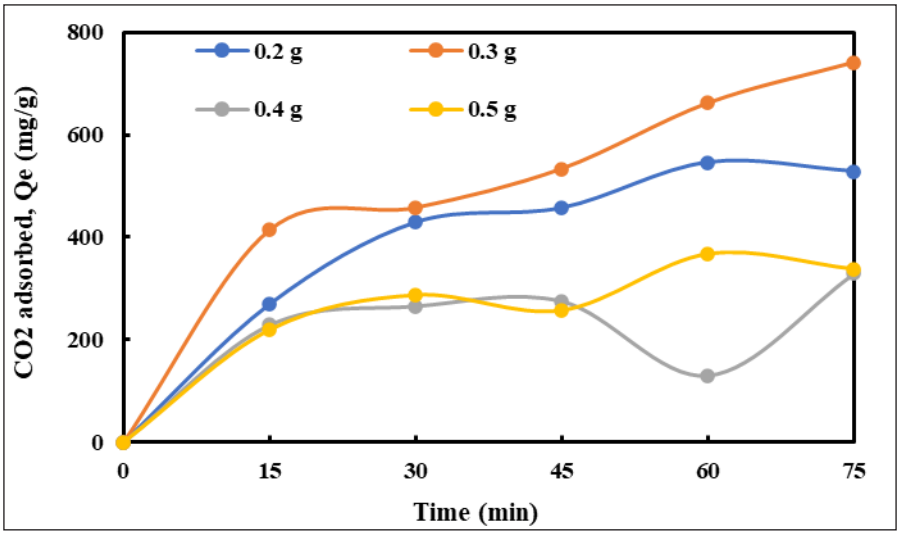

Figure 8. Influence of adsorbent dosage on the CO_2 adsorption process. Initial condition: initial pressure = 5 bar, initial concentration of CO_2 = 637 ppm, metal loading = 50 wt. % Zn/50 wt. % Mg-MOF and ambient temperature

% (338.54 mg/g). Thus, 0.3 g would be the best dosage of prepared bimetallic adsorbent as it has the highest adsorption capacity within 75 minutes of adsorption time.

Based on the findings illustrated in Figure 8, radical transformations are not observed when raising the dosage of the adsorbent. As adsorbents increase, the ability to adsorb CO_2 decreases while all other variables remain constant, as shown in Figure 8. It could be because the quantity of active sites is greater with smaller adsorbent doses. Increasing the adsorbent dose leads to the accumulation of particulate matter. As a result, the presence of adsorption sites may decrease due to reduced CO_2 adsorption capacity (Dien, 2019). It is in line with the conclusions made by Niyousha et al. (2020) and Nsami et al. (2013). The pore-clogging effect becomes more noticeable as the adsorbent dosage increases. The CO_2 uptake was decreased by the pore-blockage effect and poor diffusion caused by the higher adsorbent dose, which is because of the active phase layer of the adsorbent (Fatima et al., 2022). Smaller doses result in greater contact between the functional groups of the adsorbent and CO_2, and the support substantially influences physisorption. CO_2 particles have a higher affinity for anions (-OH and -COOH) of adsorbents (Torrisi et al., 2010). Due to the larger number of [OH] or $[COOH]^-$ anion present, the highest surface coverage was achieved with a lower load. The surface area deteriorated with a greater adsorbent dose, and the adsorbent's influence on physisorption was also insignificant. Thus, the CO_2 uptake was observed to be less effective at higher adsorbent dosages. The best performance was achieved with 0.3 g of adsorbent dosage for 50 wt.% Zn/50 wt.% Mg-MOF.

CONCLUSION

This study prepared single and bimetallic-based Metal-Organic Frameworks (MOFs) containing Zn and Mg using the impregnation method. The properties of the respective MOFs characterise the prepared MOFs. For instance, its crystalline configuration is well-maintained, the characteristic crystalline phase is recognisable, and the characteristics show the existence of bimetal (varies in surface area). 50 wt.% Zn-50 wt.% Mg-MOF adsorbent is the most favourable for CO_2 uptake. In our study, the addition of bimetal to pristine MOF (Zn-MOF or Mg-MOF-74) enhances the adsorbed CO_2 amount by 59%–62% obtained in this study. Overall, comparing the single and bimetallic MOFs, it can be summarised that bimetallic MOFs can be regarded as the most promising, as 50 wt.% Zn-50 wt.% Mg-MOF shows higher CO_2 uptake capability relative to pristine MOFs. Moreover, the proportion of bimetal used in MOF, working pressure, and adsorbent quantity all have a significant impact on the CO_2 uptake of the solid adsorbent.

ACKNOWLEDGEMENT

The Ministry of Higher Education funded the Fundamental Research Grant Scheme (FRGS) that supported this work (No. FRGS/1/2021/TK0/UMP/02/79 (University reference

RDU210150)). The authors express their gratitude to the Faculty of Chemical and Process Engineering Technology, Universiti Malaysia Pahang Al-Sultan Abdullah (UMPSA), for their technical assistance and facilities in completing this study.

REFERENCES

Abednatanzi, S., Derakhshandeh, P. G., Depauw, H., Coudert, F. X., Vrielinck, H., Van Der Voort, P., & Leus, K. (2019). Mixed-metal metal–organic frameworks. *Chemical Society Reviews*, *48*(9), 2535-2565. https://doi.org/10.1039/C8CS00337H

Abooali, D., Soleimani, R., & Rezaei-Yazdi, A. (2020). Modeling CO_2 absorption in aqueous solutions of DEA, MDEA, and DEA+ MDEA based on intelligent methods. *Separation Science and Technology*, *55*(4), 697-707. https://doi.org/10.1080/01496395.2019.1575415

Bagheri, N., Khataee, A., Habibi, B., & Hassanzadeh, J. (2018). Mimetic ag nanoparticle/zn-based MOF nanocomposite (AgNPs@ZnMOF) capped with molecularly imprinted polymer for the selective detection of patulin. *Talanta, 179*, 710-718. https://doi.org/10.1016/j.talanta.2017.12.009

Bao, Z., Yu, L., Dou, T., Gong, Y., Zhang, Q., Ren, Q., Lu, X., & Deng, S. (2011). Adsorption equilibria of CO_2, CH_4, N_2, O_2, and Ar on high silica zeolites. *Journal of Chemical & Engineering Data*, *56*(11), 4017-4023. https://doi.org/10.1021/je200394p

Bao, Z., Yu, L., Ren, Q., Lu, X., & Deng, S. (2011). Adsorption of CO_2 and CH_4 on a magnesium-based metal organic framework. *Journal of colloid and interface science*, *353*(2), 549-556. https://doi.org/10.1016/j.jcis.2010.09.065

Barea, E., Montoro, C., & Navarro, J. A. R. (2014). Toxic gas removal–metal–organic frameworks for the capture and degradation of toxic gases and vapours. *Chemical Society Reviews*, *43*(16), 5419-5430. https://doi.org/10.1039/C3CS60475F

Botas, J. A., Calleja, G., Sanchez-Sanchez, M., & Orcajo, M. G. (2011). Effect of Zn/Co ratio in MOF-74 type materials containing exposed metal sites on their hydrogen adsorption behaviour and on their band gap energy. *International Journal of Hydrogen Energy*, *36*(17), 10834-10844. https://doi.org/10.1016/j.ijhydene.2011.05.187

Campbell, J., & Tokay, B. (2017). Controlling the size and shape of Mg-MOF-74 crystals to optimise film synthesis on alumina substrates. *Microporous and Mesoporous Materials, 251*, 190-199. https://doi.org/10.1016/j.micromeso.2017.05.058

Chen, Y., Lv, D., Wu, J., Xiao, J., Xi, H., Xia, Q., & Li, Z. (2017). A new MOF 505@GO composite with high selectivity for CO_2/CH_4 and CO_2/N_2 separation. *Chemical Engineering Journal, 308*, 1065-1072. https://doi.org/10.1016/j.cej.2016.09.138

Choi, J., Im, J., Noh, K., Kim, J., Vogt, T., & Lee, Y. (2019). Universal gas-uptake behavior of a zeolitic imidazolate framework ZIF-8 at high pressure. *The Journal of Physical Chemistry C*, *123*(42), 25769-25774. https://doi.org/10.1021/acs.jpcc.9b08539

Cui, X., Yang, Q., Xiong, Y., Bao, Z., Xing, H., & Dai, S. (2017). Preparation of ordered N-doped mesoporous carbon materials via a polymer–ionic liquid assembly. *Chemical Communications*, *53*(36), 4915-4918. https://doi.org/10.1039/C7CC01000A

Deegan, M. M., Antonio, A. M., Taggart, G. A., & Bloch, E. D. (2021). Manipulating solvent and solubility in the synthesis, activation, and modification of permanently porous coordination cages. *Coordination Chemistry Reviews*, *430*, Article 213679. https://doi.org/10.1016/j.ccr.2020.213679

Dien, N. D. (2019). Preparation of various morphologies of ZnO nanostructure through wet chemical methods. *Advanced Material Science, 4*, Article 147. https://doi.org/10.15761/AMS.1000147

Fatima, S. S., Borhan, A., Ayoub, M., & Ghani, N. A. (2022). CO_2 adsorption performance on surface-functionalized activated carbon impregnated with pyrrolidinium-based ionic liquid. *Processes*, *10*(11), Article 2372. https://doi.org/10.3390/pr10112372

Gao, Z., Liang, L., Zhang, X., Xu, P., & Sun, J. (2021). Facile one-pot synthesis of Zn/Mg-MOF-74 with unsaturated coordination metal centers for efficient CO_2 adsorption and conversion to cyclic carbonates. *ACS Applied Materials & Interfaces*, *13*(51), 61334-61345. https://doi.org/10.1021/acsami.1c20878

Giordano, V. M., Datchi, F., & Dewaele, A. (2006). Melting curve and fluid equation of state of carbon dioxide at high pressure and high temperature. *The Journal of Chemical Physics*, *125*(5), Article 054504. https://doi.org/10.1063/1.2215609

Heravi, M. M., Ghavidel, M., & Mohammadkhani, L. (2018). Beyond a solvent: Triple roles of dimethylformamide in organic chemistry. *RSC advances*, *8*(49), 27832-27862. https://doi.org/10.1039/C8RA04985H

Howarth, A. J., Katz, M. J., Wang, T. C., Platero-Prats, A. E., Chapman, K. W., Hupp, J. T., & Farha, O. K. (2015). High efficiency adsorption and removal of selenate and selenite from water using metal–organic frameworks. *Journal of the American Chemical Society*, *137*(23), 7488-7494. https://doi.org/10.1021/jacs.5b03904

Hu, Y., Lin, B., He, P., Li, Y., Huang, Y., & Song, Y. (2015). Probing the structural stability of and enhanced CO_2 Storage in MOF MIL-68 (In) under high pressures by FTIR spectroscopy. *Chemistry–A European Journal*, *21*(51), 18739-18748. https://doi.org/10.1002/chem.201502980

Hu, Y., Liu, Z., Xu, J., Huang, Y., & Song, Y. (2013). Evidence of pressure enhanced CO_2 storage in ZIF-8 probed by FTIR spectroscopy. *Journal of the American Chemical Society*, *135*(25), 9287-9290. https://doi.org/10.1021/ja403635b

Jiang, S., Hu, Y., Chen, S., Huang, Y., & Song, Y. (2018). Elucidation of the structural origins and contrasting guest–host interactions in CO_2-loaded CdSDB and PbSDB metal–Organic frameworks at high pressures. *Chemistry–A European Journal*, *24*(72), 19280-19288. https://doi.org/10.1002/chem.201804069

Kahr, J., Morris, R. E., & Wright, P. A. (2013). A post-synthetic incorporation of nickel into CPO-27(Mg) to give materials with enhanced permanent porosity. *CrystEngComm, 15*(45), 9779-9786. https://doi.org/10.1039/C3CE41228H

Kaur, G., Rai, R. K., Tyagi, D., Yao, X., Li, P. Z., Yang, X. C., Zhao, Y., Xu, Q., & Singh, S. K. (2016). Room-temperature synthesis of bimetallic Co–Zn based zeolitic imidazolate frameworks in water for enhanced CO_2 and H_2 uptakes. *Journal of Materials Chemistry A*, *4*(39), 14932-14938. https://doi.org/10.1039/C6TA04342A

Kim, A. R., Yoon, T. U., Kim, S. I., Cho, K., Han, S. S., & Bae, Y. S. (2018). Creating high CO/CO_2 selectivity and large CO working capacity through facile loading of Cu (I) species into an iron-based mesoporous

metal-organic framework. *Chemical Engineering Journal*, *348*, 135-142. https://doi.org/10.1016/j.cej.2018.04.177

Kontos, A. G., Romanos, G. E., Veziri, C. M., Gotzias, A., Arfanis, M. K., Kouvelos, E., Likodimos, V., Naranikolos, G. G., & Falaras, P. (2020). Correlating vibrational properties with temperature and pressure dependent CO_2 adsorption in zeolitic imidazolate frameworks. *Applied Surface Science*, *529*, Article 147058. https://doi.org/10.1016/j.apsusc.2020.147058

Lee, W. H., Zavgorodniy, A. V., Loo, C. Y., & Rohanizadeh, R. (2012). Synthesis and characterization of hydroxyapatite with different crystallinity: Effects on protein adsorption and release. *Journal of Biomedical Materials Research Part A*, *100*(6), 1539-1549. https://doi.org/10.1002/jbm.a.34093

Li, H., Meng, B., Mahurin, S. M., Chai, S. H., Nelson, K. M., Baker, D. C., Liu, H., & Dai, S. (2015). Carbohydrate based hyper-crosslinked organic polymers with–OH functional groups for CO_2 separation. *Journal of Materials Chemistry A*, *3*(42), 20913-20918. https://doi.org/10.1039/C5TA03213J

Li, H., Yang, Z., Lu, S., Su, L., Wang, C., Huang, J., Zhou, J., Tang, J., & Huang, M. (2021). Nano-porous bimetallic CuCo-MOF-74 with coordinatively unsaturated metal sites for peroxymonosulfate activation to eliminate organic pollutants: Performance and mechanism. *Chemosphere*, *273*, Article 129643. https://doi.org/10.1016/j.chemosphere.2021.129643

Li, L. (2021). *Synthesis and catalytic properties of metal-organic frameworks mimicking carbonic anhydrase*. [Doctoral dissertation]. Western Kentucky University, USA. https://digitalcommons.wku.edu/stu_hon_theses/924

Ling, J., Zhou, A., Wang, W., Jia, X., Ma, M., & Li, Y. (2022). One-pot method synthesis of bimetallic MgCu-MOF-74 and its CO_2 adsorption under visible light. *Acs Omega*, *7*(23), 19920-19929. https://doi.org/10.1021/acsomega.2c01717

Liu, Y., Ghimire, P., & Jaroniec, M. (2019). Copper benzene-1, 3, 5-tricarboxylate (Cu-BTC) metal-organic framework (MOF) and porous carbon composites as efficient carbon dioxide adsorbents. *Journal of colloid and interface science*, *535*, 122-132. https://doi.org/10.1016/j.jcis.2018.09.086

Luo, F., Chen, J. L., Dang, L. L., Zhou, W. N., Lin, H. L., Li, J. Q., Liu, S. J., & Luo, M. B. (2015). High-performance Hg^{2+} removal from ultra-low-concentration aqueous solution using both acylamide-and hydroxyl-functionalized metal–organic framework. *Journal of Materials Chemistry A*, *3*(18), 9616-9620. https://doi.org/10.1039/C5TA01669J

Masoomi, M. Y., Morsali, A., Dhakshinamoorthy, A., & Garcia, H. (2019). Mixed-metal MOFs: unique opportunities in metal–organic framework (MOF) functionality and design. *Angewandte Chemie*, *131*(43), 15330-15347. https://doi.org/10.1002/ange.201902229

Moggach, S. A., Bennett, T. D., & Cheetham, A. K. (2009). The effect of pressure on ZIF-8: increasing pore size with pressure and the formation of a high-pressure phase at 1.47 GPa. *Angewandte Chemie International Edition*, *48*(38), 7087-7089. https://doi.org/10.1002/anie.200902643

Niyousha, K. M., Ahad, G., Kambiz, T., & Mehrdad S. A. A. (2020). Experimental investigation and modeling of CO_2 adsorption using modified activated carbon. Iranian *Journal of Chemistry and Chemical Engineering, 39(1)*, 177-192.

Nsami, J. N., & Mbadcam, J. K. **(2013)**. The adsorption efficiency of chemically prepared activated carbon from cola nut shells by $ZnCl_2$ on methylene blue. *Journal of Chemistry, 2013*, Article 469170. http://dx.doi.org/10.1155/2013/469170

Ren, W., Wei, Z., Xia, X., Hong, Z., & Li, S. (2020). CO_2 adsorption performance of CuBTC/graphene aerogel composites. *Journal of Nanoparticles Research, 22*, Article 191. https://doi.org/10.1007/s11051-020-04933-4

Romero-Muñiz, C., Gavira-Vallejo, J. M., Merkling, P. J., & Calero, S. (2020). Impact of small adsorbates in the vibrational spectra of Mg-and Zn-MOF-74 revealed by first-principles calculations. *ACS Applied Materials & Interfaces*, *12*(49), 54980-54990. https://doi.org/10.1021/acsami.0c16629

Saha, D., Bramer, S. E. V., Orkoulas, G., Ho, H. C., Chen, J., & Henley, D. K. (2017). CO2 capture in lignin-derived and nitrogen-doped hierarchical porous carbons. *Carbon*, *121*, 257-266. https://doi.org/10.1016/j.carbon.2017.05.088

Serre, C., Bourrelly, S., Vimont, A., Ramsahye, N. A., Maurin, G., Llewellyn, P. L., Daturi, M., Filinchuk, Y., Leynaud, O., Barnes, P., & Férey, G. (2007). An explanation for the very large breathing effect of a metal-organic framework during CO_2 adsorption. *Advanced Materials, 19*(17), 2246-2251. https://doi.org/10.1002/adma.200602645

Sillar, K., & Sauer, J. (2012). Ab initio prediction of adsorption isotherms for small molecules in metal–organic frameworks: the effect of lateral interactions for methane/CPO-27-Mg. *Journal of the American Chemical Society*, *134*(44), 18354-18365. https://doi.org/10.1021/ja307076t

Sumida, K., Rogow, D. L., Mason, J. A., McDonald, T. M., Bloch, E. D., Herm, Z. R., Bae, T. H., & Long, J. R. (2012). Carbon dioxide capture in metal-organic frameworks. *Chemical Reviews, 112*(2), 724-781. https://doi.org/10.1021/cr2003272

Sun, H., Ren, D., Kong, R., Wang, D., Jiang, H., Tan, J., Wu, D., Chen, S., & Shen, B. (2019). Tuning 1-hexene/n-hexane adsorption on MOF-74 via constructing Co-Mg bimetallic frameworks. *Microporous and Mesoporous Materials*, *284*, 151-160. https://doi.org/10.1016/j.micromeso.2019.04.031

Szczesniak, B., Choma, J., & Jaroniec, M. (2018). Gas adsorption properties of hybrid graphene-MOF materials. *Journal of Colloid and Interface Science, 514*, 801-813. https://doi.org/10.1016/j.jcis.2017.11.049

Tan, K., Zuluaga, S., Gong, Q., Canepa, P., Wang, H., Li, J., Chabal, Y. J., Thonhauser, T. (2014). Water reaction mechanism in metal organic frameworks with coordinatively unsaturated metal ions: MOF-74. *Chemistry of Materials, 26*(23), 6886-6895. https://doi.org/10.1021/cm5038183

Tapiador, J., Leo, P., Rodríguez-Diéguez, A., Choquesillo-Lazarte, D., Calleja, G., & Orcajo, G. (2022). A novel Zn-based-MOF for efficient CO_2 adsorption and conversion under mild conditions. *Catalysis Today*, *390-391*, 230-236. https://doi.org/10.1016/j.cattod.2021.11.025

Torrisi, A., Bell, R. G., Mellot-Draznieks, C. (2010). Functionalized MOFs for enhanced CO_2 capture. *Crystal Growth & Design,10*(7), 2839-2841. https://doi.org/10.1021/cg100646e

Valenzano, L., Civalleri, B., Chavan, S., Bordiga, S., Nilsen, M. H., Jakobsen, S., Lillerud, J. P., & Lamberti, C. (2011). Disclosing the complex structure of UiO-66 metal organic framework: A synergic combination of experiment and theory. *Chemistry of Materials, 23*(7), 1700-1718. https://doi.org/10.1021/cm1022882

Villajos, J. A., Orcajo, G., Martos, C., Botas, J. Á., Villacañas, J., & Calleja, G. (2015). Co/Ni mixed-metal sited MOF-74 material as hydrogen adsorbent. *International Journal of Hydrogen Energy*, *40*(15), 5346-5352. https://doi.org/10.1016/j.ijhydene.2015.01.113

Vo, T. K., Bae, Y. S., Chang, B. J., Moon, S. Y., Kim, J. H., & Kim, J. (2019). Highly CO selective Cu (I)-doped MIL-100 (Fe) adsorbent with high CO/CO2 selectivity due to π complexation: Effects of Cu (I) loading and activation temperature. *Microporous and Mesoporous Materials*, *274*, 17-24. https://doi.org/10.1016/j.micromeso.2018.07.024

Vuong, G. T., Pham, M. H., & Do, T. O. (2013). Synthesis and engineering porosity of a mixed metal Fe_2 Ni MIL-88B metal–organic framework. *Dalton Transactions*, *42*(2), 550-557. https://doi.org/10.1039/C2DT32073H

Wang, J., Cui, S., Li, Z., Wen, S., Ning, P., Lu, S., Lu, P., Huang, L., & Wang, Q. (2021). Comprehensive investigation of dynamic CO_2 capture performance using Mg/DOBDC as precursor to fabricate a composite of metallic organic framework and graphene oxide. *Chemical Engineering Journal*, *415*, Article 128859. https://doi.org/10.1016/j.cej.2021.128859

Wang, J., Huang, J., Wu, X., Yuan, B., Sun, Y., Zeng, Z., & Deng, S. (2014). Effect of nitrogen group on selective separation of CO_2/N_2 in porous polystyrene. *Chemical Engineering Journal*, *256*, 390-397. https://doi.org/10.1016/j.cej.2014.06.104

Wang, J., Yang, J., Krishna, R., Yang, T., & Deng, S. (2016). A versatile synthesis of metal–organic framework-derived porous carbons for CO_2 capture and gas separation. *Journal of Materials Chemistry A*, *4*(48), 19095-19106. https://doi.org/10.1039/C6TA07330A

Wu, H., Simmons, J. M., Srinivas, G., Zhou, W., & Yildirim, T. (2010). Adsorption sites and binding nature of CO_2 in prototypical metal− organic frameworks: a combined neutron diffraction and first-principles study. *The Journal of Physical Chemistry Letters*, *1*(13), 1946-1951. https://doi.org/10.1021/jz100558r

Xie, S., Qin, Q., Liu, H., Jin, L., Wei, X., Liu, J., Liu, X., Yao, Y., Dong, L., & Li, B. (2020). MOF-74-M (M= Mn, Co, Ni, Zn, MnCo, MnNi, and MnZn) for low-temperature NH3-SCR and in situ DRIFTS study reaction mechanism. *ACS Applied Materials & Interfaces*, *12*(43), 48476-48485. https://doi.org/10.1021/acsami.0c11035

Xin, L. Y., Liu, G. Z., Li, X. L., & Wang, L. Y. (2011). Structural Diversity for a Series of Metal(II) Complexes Based on Flexible 1,2-Phenylenediacetate and Dipyridyl-type Coligand. *Crystal Growth & Design, 12*(1), 147-157. https://doi.org/10.1021/cg200903k

Yang, J., Li, J., Wang, W., Li, L., & Li, J. (2013). Adsorption of CO2, CH4, and N2 on 8-, 10-, and 12-membered ring hydrophobic microporous high-silica zeolites: DDR, silicalite-1, and beta. *Industrial & Engineering Chemistry Research*, *52*(50), 17856-17864. https://doi.org/10.1021/ie403217n

Yang, J., Zheng, C., Xiong, P., Li, Y., & Wei, M. (2014). Zn-doped Ni-MOF material with a high supercapacitive performance. *Journal of Materials Chemistry A*, *2*(44), 19005-19010. https://doi.org/10.1039/C4TA04346D

Yazaydin, A. O., Snurr, R. Q., Park, T. H., Koh, K., Liu, J., Levan, M. D., Benin, A. I., Jakubczak, P., Lanuza, M., Galloway, D. B., Low, J. J., & Willis, R. R. (2009). Screening of metal-organic frameworks for carbon dioxide capture from flue gas using a combined experimental and modeling approach. *Journal of the American Chemical Society*, *131*(51), 18198-18199.

Yu, C. H., Huang, C. H., & Tan, C. S. (2012). A review of CO_2 capture by absorption and adsorption. *Aerosol and Air Quality Research*, *12*(5), 745-769. https://doi.org/10.4209/aaqr.2012.05.0132

Zhang, Z., Liu, J., Wang, Z., & Zhang, J. (2020). Bimetallic Fe–Cu-based metal–organic frameworks as efficient adsorbents for gaseous elemental mercury removal. *Industrial & Engineering Chemistry Research*, *60*(1), 781-789. https://doi.org/10.1021/acs.iecr.0c04298

Zhou, W., Wu, H., & Yildirim, T. (2008). Enhanced H_2 adsorption in isostructural metal− organic frameworks with open metal sites: Strong dependence of the binding strength on metal ions. *Journal of the American Chemical Society*, *130*(46), 15268-15269. https://doi.org/10.1021/ja807023q

Zhu, X. W., Zhou, X. P., & Li, D. (2016). Exceptionally water stable heterometallic gyroidal MOFs: tuning the porosity and hydrophobicity by doping metal ions. *Chemical Communications*, *52*(39), 6513-6516. https://doi.org/10.1039/C6CC02116F

Zou, R., Li, P. Z., Zeng, Y. F., Liu, J., Zhao, R., Duan, H., Luo, Z., Wang, J. G., Zou, R., & Zhao, Y. (2016). Bimetallic metal-organic frameworks: Probing the lewis acid site for CO_2 conversion. *Small*, *12*(17), 2334-2343. https://doi.org/10.1002/smll.201503741

Zurrer, T., Wong, K., Horlyck, J., Lovell, E. C., Wright, J., Bedford, N. M., Han, K., Scott, J., & Amal, R. (2021). Mixed-metal MOF-74 templated catalysts for efficient carbon dioxide capture and methanation. *Advanced Functional Materials*, *31*(9), Article 2007624. https://doi.org/10.1002/adfm.202007624